

Molecular cloning and functional analysis of two phosphate transporter genes from *Rhizopogon luteolus* and *Leucocortinarius bulbiger*, two ectomycorrhizal fungi of *Pinus tabulaeformis*

Rong Zheng^{1,2} · Jugang Wang^{1,3} · Min Liu¹ · Guozhen Duan¹ · Xiaomin Gao³ · Shulan Bai¹ · Yachao Han⁴

Received: 1 November 2015 / Accepted: 14 April 2016 / Published online: 21 April 2016
© Springer-Verlag Berlin Heidelberg 2016

Abstract Inorganic phosphorus (Pi) is essential for plant growth, and phosphate (P) deficiency is a primary limiting factor in *Pinus tabulaeformis* development in northern China. P acquisition in mycorrhizal plants is highly dependent on the activities of phosphate transporters of their root-associated fungi. In the current study, two phosphate transporter genes, *RIPT* and *LbPT*, were isolated from *Rhizopogon luteolus* and *Leucocortinarius bulbiger*, respectively, two ectomycorrhizal fungi forming symbiotic interactions with the *P. tabulaeformis*. Phylogenetic analysis suggested that the sequence of the phosphate transporter of *L. bulbiger* is most closely related to a phosphate transporter of *Hebeloma cylindrosporum*, whereas the phosphate transporter of *R. luteolus* is most closely related to that of *Piloderma croceum*. The subcellular localization indicated that *RIPT* and *LbPT* were expressed in the plasma membrane. The complementation assay in yeast indicated that both *RIPT*

and *LbPT* partially compensated for the absence of phosphate transporter activity in the MB192 yeast strain, with a K_m value of 57.90 $\mu\text{mol/L}$ Pi for *RIPT* and 35.87 $\mu\text{mol/L}$ Pi for *LbPT*. qPCR analysis revealed that *RIPT* and *LbPT* were significantly up-regulated at lower P availability, which may enhance P uptake and transport under Pi starvation. Our results suggest that *RIPT* and *LbPT* presumably play a key role in Pi acquisition by *P. tabulaeformis* via ectomycorrhizal fungi.

Keywords Phosphate transporter · Ectomycorrhizae · Heterologous characterization · Gene expression · *Pinus tabulaeformis*

Introduction

Plants, such as wheat, require at least 16 macro- and micro-nutrients for their growth and reproduction (Miransari and Mackenzie 2011); among these nutrients, phosphorus (P) is one of the limiting factors that influence forest productivity and crop yields. In addition, P is particularly important for plant water uptake. It has been known for some time that the hydraulic conductivity of intact roots and root cortical cells is lower under P deficiency (Faustino et al. 2013). In soil, concentrations of free inorganic orthophosphate (Pi), which is the only form of P directly accessible to plants, are often very low, generally ranging from 1 to 10 $\mu\text{mol/L}$. The low availability of Pi in soil is due to the negative charges on orthophosphate that result in rapid sequestration by cations (Vance et al. 2003), which renders Pi highly immobile in soil (Hinsinger 2001). Thus, the uptake of phosphate by plant roots quickly generates a depletion zone. Consequently, supplementation and/or maintenance of the P supply is important to ensuring normal plant growth.

Rong Zheng and Jugang Wang contributed equally to this work.

Electronic supplementary material The online version of this article (doi:10.1007/s00572-016-0702-7) contains supplementary material, which is available to authorized users.

✉ Shulan Bai
baishulan2004@163.com

¹ College of Forestry, Inner Mongolia Agricultural University, Hohhot 010019, Inner Mongolia, China

² College of Life Science and Technology, Inner Mongolia Normal University, Hohhot 010020, Inner Mongolia, China

³ South Subtropical Crops Research Institute, Chinese Academy of Tropical Agricultural Science, Zhanjiang 524091, Guangdong, China

⁴ Fuyang Vocational and Technical College, Fuyang 236031, Anhui, China

Mycorrhizal symbiosis is widely distributed in terrestrial ecosystems (Smith and Read 2008) and occupies a protected ecological niche by improving host plant nutrient uptake, especially P uptake (de Campos et al. 2013). It is well established that mycorrhizal plants have two pathways of P absorption: a direct uptake pathway through the epidermis and root hairs and a mycorrhizal uptake pathway, in which P absorbed by external fungal hyphae is translocated to structures inside the roots and thus across the symbiotic interface to the plant cortical cells (Bucher 2007; Stonor et al. 2014). In most cases, plants cannot obtain enough P via the direct uptake pathway because of low P availability in the rhizosphere; consequently, P absorption by host plants has been shown to rely heavily on the mycorrhizal uptake pathway (Smith and Smith 2012).

In the mycorrhizal uptake pathway, a high-affinity phosphate transporter (PT) of mycorrhizal fungi plays an important role (Rausch and Bucher 2002), and many partial or full-length cDNAs codes for mycorrhizal PTs have been identified. Harrison and van Buuren (1995) first cloned a PT from the arbuscular mycorrhizal fungus *Diversispora epigaea* and then cloned the PT genes of *Rhizophagus intraradices* (Maldonado-Mendoza et al. 2001) and *Funneliformis mosseae* (Benedetto et al. 2005). In 2011, Sokolski et al. (2011) obtained 25 PT gene fragments from 10 species of arbuscular mycorrhizal fungi by using 4 pairs of special primers (P3, P4, P6, and P7). For ectomycorrhizal (ECM) fungi, the PT genes of *Boletus edulis* (Wang et al. 2014), *Hebeloma cylindrosporum* (Tatry et al. 2009), *Laccaria bicolor* (Martin et al. 2008), *Pholiota nameko* (Tasaki et al. 2002), and *Tuber melanosporum* (Martin et al. 2010) have been characterized. In the ongoing project entitled “Exploring the genome diversity of mycorrhizal fungi to understand the evolution and functioning of symbiosis in woody shrubs and trees,” at least 34 PT genes of 11 ECM fungi species, including *Amanita muscaria*, *Laccaria amethystine*, *Paxillus involutus*, *Paxillus rubicundulus*, *Piloderma croceum*, *Pisolithus microcarpus*, *Pisolithus tinctorius*, *Scleroderma citrinum*, *Sebacina vermifera*, *Suillus luteus*, and *Tulasnella calospora*, were retrieved from the Joint Genome Institute (JGI, (<http://genome.jgi-psf.org/>)) database (Casieri et al. 2013). These fungal PTs are of great benefit to their host plants by absorbing P from outside of the P depletion zone (Facelli et al. 2014).

Pinus tabulaeformis is a dominant species of coniferous tree in northern China (Chen et al. 2008) and has been widely planted in protected forests and landscape enhancement projects (Bai et al. 2009). However, P deficiency in northern China (Yan et al. 2006) negatively affects the growth, development, and spatial distribution of *P. tabulaeformis* trees, resulting in substantial losses. Furthermore, *P. tabulaeformis* is a typical mycorrhizal plant that shows high dependence on the ectomycorrhizae (Bai et al. 2009; Wu et al. 1999; Zhang et al. 2010). Our previous study indicated that inoculation with *Rhizopogon luteolus* and

Leucocortinarius bulbiger significantly improves the growth status and P absorption of *P. tabulaeformis* seedlings (Bai et al. 2009). Therefore, understanding the mechanism underlying P uptake and use efficiency along with ECM interactions is critical for *P. tabulaeformis* in northern China. Although many ECM fungal high-affinity PTs have been predicted or identified, most ECM fungi species develop specific associations with their host plants (Roy et al. 2013). Unfortunately, there is no information in the literature on the PT of *P. tabulaeformis*' native ECM fungi. In the present study, two high-affinity PT genes were cloned, identified, and functionally characterized from *R. luteolus* and *L. bulbiger*.

Materials and methods

Strains, plasmids, and culture conditions

Two fungal strains were originally isolated from the mixed coniferous-broadleaved *P. tabulaeformis* forest on Daqingshan Mountain, Inner Mongolia, northern China (longitude 109° 41' E to 112° 17' E, latitude 40° 34' N to 41° 14' N) in August 2004. The strains were well maintained, and more than 40 generations were transferred in modified Melin Norkans medium (MMN, Boon et al. 2000). Based on the fungal sporocarp morphology described by Mao (2009), these two strains were identified as *R. luteolus* and *L. bulbiger*. The sporocarp morphology and ECM characteristics (associated with the *P. tabulaeformis*) are shown in Fig. S1, and the internal transcribed spacer (ITS) sequences of these two fungi species were deposited in the National Center for Biotechnology Information (NCBI, <http://www.ncbi.nlm.nih.gov/>) and are accessible using the following accession numbers: KC984860 for *R. luteolus* and KC984861 for *L. bulbiger*. The mycelia of *R. luteolus* and *L. bulbiger* were incubated in MMN medium at 25 °C for 20 days and collected for RNA and DNA extraction and gene cloning. *Escherichia coli* DH5 α was used for the Luria-Bertani (LB) medium transformation (Sezonov et al. 2007) at 37 °C. Yeast strains, including a wild-type (WT) strain and the corresponding mutant MB192 (MA *Tapho3-1* Δ *pho84:HIS3 ade2 leu2-3,112 his3-532 trp1-289ura3-1,2 can1*), were grown in both a yeast extract peptone dextrose medium (1 % yeast extract and 2 % peptone supplemented with 2 % glucose) and a synthetic defined medium (6.7 g/L of a yeast nitrogen base without Pi, contained all of the amino acid supplements, and supplemented with a 200 mg/L geneticin (G418)) at 30 °C. The pUG23 vector with a KanMx-tag was used for the heterogeneous expression of the *RIPT* and *LbPT* gene in yeast. The modified pUG23 vector with a cleavable green fluorescent protein gene (*GFP*) and a KanMx-tag was used for the subcellular localization of the *RIPT* and *LbPT* in yeast. The pMD18-T Simple Vector (TaKaRa, Dalian,

China) was used for thymine and adenine (TA) cloning and DNA sequencing.

Gene cloning and bioinformatic analysis

Nucleic acid extraction and cDNA synthesis

The total RNAs were prepared using an RNA Easy Spin Plus Kit (Aidlab, Beijing, China) from approximately 0.5 g fresh mycelia of two strains according to the manufacturer's protocol. Then, the quantity and purity of the RNA were determined by UV measurement (NanoDrop 2000c spectrophotometer, Thermo Scientific, Loughborough, UK) and 1.2 % agarose gel electrophoresis. First-strand cDNAs were synthesized from the total RNA using a Revert Aid First-Strand cDNA synthesis Kit (Thermo, Shanghai, China). The synthesized first-strand cDNAs were used as a PCR template as in the following description. The genomic DNA was prepared using a DP305 Plant Genomic DNA Kit (Tiangen, Beijing, China) according to the manufacturer's protocol.

Cloning the RIPT and LbPT genes

Based on degenerate primers (see Table S1) designed from the published *PT* sequence alignments of cDNA contigs, the core fragments of *RIPT* and *LbPT* were amplified from the cDNA templates using touchdown PCR conditions. In total, the 50- μ L PCR mixture contained 5 μ L PCR buffer, 3 μ L dNTP mixture (2 mmol/L), 4 μ L degenerate primers (5 mmol/L each), 0.5 μ L Taq DNA Polymerase (Toyobo, Shanghai, China), 5 μ L cDNA template (2.5 ng), and 32.5 μ L ddH₂O. The thermal cycler (Eppendorf AG 22331, Hamburg, Germany) was programmed for touchdown PCR with denaturation at 94 °C for 4 min, followed by 35 cycles of the following three steps: denaturation at 94 °C for 30 s, annealing at 55 °C for 30 s, and extension at 72 °C for 1 min. The PCR ended with an extra extension of 10 min at 72 °C. Then, the PCR products were purified using a BioTeke Gel Extraction Kit (BioTeke, Beijing, China). The fragment was cloned into the pMD18-T Simple Cloning Vector (TaKaRa, Dalian, China) and transformed into competent *E. coli* DH5 α for DNA sequencing. The rapid amplification of cDNA end (RACE) technique was applied to determine the full-length sequence based on the obtained cDNA core fragments using the 5' RACE system (version 2.0, Invitrogen, USA) and a SMART^{cr} RACE cDNA Amplification kit (Clontech, CA, USA). After 5' and 3' RACE, PCR was performed with high-fidelity KOD FX (Toyobo, Shanghai, China) using the primers *RIPT* full length and *LbPT* full length (Table S1) to obtain the full-length genes.

Bioinformatic analysis

The open reading frame (ORF) was predicted using the ORFfinder (<http://www.ncbi.nlm.nih.gov/gorf/orf.cgi>). The cloned *RIPT* and *LbPT* were analyzed to predict the amino acid sequences using the DNAMAN software package (version 7.0.2.176, LynnonBioSoft, Canada). The analyses of the amino acid sequences of *RIPT* and *LbPT* were performed using protein Basic Local Alignment Search Tool (BLAST) (<http://www.ncbi.nlm.nih.gov/BLAST>) algorithms. The predicted amino acid sequences were used to search for conserved domains with NCBI Conserved Domain Search database (CDD, <http://www.ncbi.nlm.nih.gov/Structure/cdd/wrpsb.cgi>). The isoelectric points (pIs) and molecular masses were predicted using the Compute pI/Mw tool from the Expert Protein Analysis System (ExPASy) database (http://www.expasy.ch/tools/pi_tool.html). The potential transmembrane domains in the protein sequences were predicted using the HMMTOP program (<http://www.enzim.hu/hmmtop/>) (Tusnady and Simon 2001), TMPred (http://www.ch.embnet.org/software/TMPRED_form.html), and the Network Protein Sequence Analysis (NPSA) (http://npsa-pbil.ibcp.fr/cgi-bin/npsa_automat.pl?page?NPSA/npsa_htm.html). The putative amino acid sequences of *RIPT* and *LbPT* and the other *PTs* from different organisms were aligned using the DNAMAN software package and the Clustal X program, version 1.83 (Thompson et al. 1997). A phylogenetic analysis was performed using the maximum likelihood method (Murshudov et al. 1997) in the MEGA5 program (Tamura et al. 2011).

Functional analysis of *RIPT* and *LbPT*

Functional complementation of yeast mutants involving RIPT and LbPT

Based on the sequences of these two *PTs* (*RIPT* and *LbPT*) and the homologous sequence of the pUG23 vector (Cormack et al. 1997) with the KnaMx marker, two pairs of specific functional verification primers (see Table S1) were designed to verify the function of *RIPT* and *LbPT*. First, the pUG23 vector was cut with a *smal* enzyme. Then, the PCR products were purified and mixed with the linear vector and the recombinant yeast expression vector pUG23+*PT* was constructed using the ClonExpress cloning Kit (Vazyme, Nanjing, China). Finally, the pUG23+*PT* vectors were transformed into MB192 yeast strains using electro-transformation (Faber et al. 1994). The WT yeast strains and the mutant strain MB192, which was transformed using the empty pUG23 vector, were used as positive and negative controls, respectively.

Transformed cells were transferred into YPD medium (Zinser et al. 1991) that contained all of the amino acid supplements with a 200-mg/L resistance concentration of G418 at

30 °C. The four yeast strains were collected during the exponential growth phase, and cells with an initial OD 600 nm of 0.5 ± 0.01 were incubated in yeast nitrogen base (YNB) medium (Chandra et al. 2001) without Pi and at 30 °C for 4 h P starvation treatment. The yeast cells were rinsed with 0.9 % NaCl solution after centrifugation at 3500 rpm for 5 min, then 2 μ L of resuspended (10 times dilution) yeast cells was dropped into the low-P (60 μ mol/L) and normal-P (200 μ mol/L) YNB medium and cultured at 30 °C; the cell growth status of each treatment was observed after 3 days. Each treatment was replicated five times.

The effects of pH on RIPT and LbPT activities in yeast

To substantiate the pH dependence of Pi uptake in the pUG23+PT, WT, and MB192 yeast strains, different extracellular pH levels, which ranged from 4.0 to 8.0, were used with 80 mmol/L Pi in YNB medium. A 2-(*N*-morpholino) ethanesulfonic acid (MES) buffer was used to maintain a stable pH value in the medium. Yeast cells with an initial OD 600 nm of 0.5 ± 0.01 were incubated in a different pH YNB medium and cultured at 30 °C for 24 h. Then, the OD 600 nm values of the yeasts were determined (Wu et al. 2011). Each treatment was replicated five times.

Subcellular localization of RIPT and LbPT in yeast

A modified pUG23 vector with a cleavable GFP and a KanMx-tag (Melikant et al. 2004) and two pairs of specific subcellular localization primers (see Table S1) were used in the subcellular localization experiment. The recombinant vector's construction and transformation, screening the positive clones and P starvation culture, were carried out as in the above description in the functional complementation experiment. The centrifuged (3500 rpm) yeast cells were incubated in a low-P (60 μ mol/L) YNB medium after treatment with P starvation. The 1,1-dioctadecyl-3,3,3,3-tetramethylindocarbocyanine perchlorate (Dil) was added to the medium to set the final concentration of Dil at 3 μ g/mL, then the medium was incubated in a water bath at 37 °C for 17 min. In order to wash the float, all aliquots were rinsed three times with the 0.9 % NaCl solution. The resuspended yeast cells (add 1 mL 0.9 % NaCl solution) were observed using a confocal laser scanning microscope (Olympus FV10, Tokyo, Japan), and the excitation wavelength was 960 nm. The transformed MB192 with the empty pUG23+GFP vector was also checked as the control.

Determination of acid phosphatase enzyme activities of RIPT and LbPT in yeast

The single clone yeast (pUG23+PT) cells were cultured in a high-P (200 μ mol/L) YNB medium at 37 °C for 36 h; then, they were centrifuged (3500 rpm) and incubated in YNB medium (without P) for 2 h of P starvation. The yeast cells that were

treated with P starvation were transferred into the same volume at different P concentrations (the final concentrations of P in each medium were 20, 60, 100, 200 μ mol/L, respectively) in YNB medium for culturing for 1 h. All of the cultures were centrifuged at 3500 rpm, after which 200 μ L of ground buffer (including 90 mmol/L citrate and 10 mmol/L chloride, pH = 4.8) was added to the fungal pellet for low-temperature grinding. The grinding mixtures were centrifuged at 15,000 rpm; then, 100 μ L of ground supernatant and 100 μ L *P*-nitrophenol sodium phosphate solution (4 mg/L) were reacted at 37 °C for 2 h; finally, a 1-mL sodium hydroxide solution (0.1 mol/L) was added to the reaction liquid to stop the reaction. The absorbance of the final reaction liquid at 420 nm wavelength was determined, as was the YNB medium without incubated yeast cells, which served as the control. A unit enzyme activity was defined as the amount of acid phosphatase needed by 1 g yeast cell to hydrolyze *P*-nitrophenol sodium phosphate to 1 μ mol/L *P*-nitrophenol for 1 min at 37 °C and pH = 4.8 (Classics-Barka and Anderson 1962).

The kinetic properties of RIPT and LbPT

The kinetic properties of RIPT and LbPT were analyzed by feeding the transformed yeast cells with 32 P, labeled Pi (Liu et al. 2014). The washed and Pi-starved cells were resuspended in a 3 % glucose solution to energize the plasma membrane. The Pi uptake by intact yeast cells was assayed by adding 2 mL of 32 P-orthophosphate (0.05 mCi; 1 mCi = 37 MBq) to 50 mL aliquots of cells, suspended in a 25-mmol/L Tris–succinate (pH = 6.5) solution, and then supplemented with 3 % glucose, resulting in final Pi concentrations varying from 0 to 100 μ mol/L in a 15-mmol/L NaCl solution. The data were analyzed using SIGMAPLOT (v10.0) to determine the K_m values of the RIPT and LbPT in Pi uptake.

Expression of two PT genes in mycelium at different Pi concentrations

Real-time reverse transcription PCR (RT-PCR) analysis, including the RIPT expression in *R. luteolus* and LbPT expression in *L. bulbiger*, was conducted in response to the addition of nutrient-enriched (5 and 10 g/L), nutrient-deficient (0.01 and 0.1 g/L), and normal (1 g/L) Pi in Ohta medium (Ohta 1990). Two ECM strains were cultured in a modified Ohta medium supplemented with 0.01, 0.1, 1, 5, and 10 g/L of KH₂PO₄ for 20 days. The fresh RNA was isolated using an RNA Easy Spin Plus Kit (Aidlab, Beijing, China) from the mycelia of each treatment, which was purified with absolute alcohol and treated with DNase (EN0521, Thermo). Real-time PCR was performed using SYBR Premix Ex Taq (TaKaRa, Dalian, China), and quantitative RT-PCR reactions were conducted using the LightCycler 480 real-time PCR system (Roche) following the manufacturer's instructions. The reaction mixture (25 μ L) contained 2 \times Maxima SYBR Green qPCR Master Mix (12.5 μ L), 1 μ mol/L each of the

forward and reverse primers (1 μL , the primers are listed in Table S1), 2 μL of template cDNA, and 9.5 μL of nuclease-free water. PCR amplification was conducted under the following conditions: 95 °C for 10 min, followed by 40 cycles at 95 °C for 15 s and 60 °C for 60 s. Three independent biological replicates of each sample and three technical replicates of each biological replicate were done in qPCR analysis. The gene expression of these two *PTs* was normalized against an internal reference gene, γ -actin (Zheng et al. 2014). The relative transcript expression was calculated using the $2^{-\Delta\Delta\text{Ct}}$ method (Livak and Schmittgen 2001).

Results

Cloning of the RIPT and LbPT

Based on degenerate primer pair and PCR amplification, we obtained two conserved region sequences, with 898 and 971 bp lengths. These two conserved region sequences exhibited significant similarity with fungal *PT* sequences from the National Center for Biotechnology Information (NCBI) (<http://www.ncbi.nlm.nih.gov>) database (data not shown). Using the 5' RACE and 3' RACE techniques, we cloned the full-length cDNA sequences of two *PTs* and named them *RIPT* with 2017 bp and *LbPT* with 1890 bp length (GenBank accession numbers were KM594556 and KM594557, respectively).

The ORF of *RIPT* consisted of 1653 bp predicted to code 550 amino acids, and the ORF of *LbPT* with 1680 bp length corresponded to 559 amino acids. Based on the amino acid sequences of two proteins, we found 52.6 % of hydrophobic and 32.1 % of hydrophilic amino acids in the *RIPT* whereas 50.6 % of hydrophobic and 35.1 % of hydrophilic amino acids in the *LbPT*. And the ExPASy online hydrophobic predications of these two proteins were also shown in Fig. S2. The pI and the calculated molecular mass were 8.376 and 59.786 kDa for *RIPT* and 7.190 and 61.26 kDa for *LbPT*, respectively. The DNA sequences of these two genes analyzed by the HTMM software revealed *RIPT* contained 11 exons and 10 introns and *LbPT* contained 16 exons and 15 introns (Fig. S3).

The results from the NCBI Conserved Domain Search further confirmed that *RIPT* and *LbPT* belong to the major facilitator superfamily (MFS). Furthermore, we found *RIPT* had 10 transmembrane-spanning (TMs) domains by using TMHMM software, and *LbPT* had 9 TMs (Fig. S4). The signal peptide prediction analysis indicated that no signal peptide sequence was observed in *RIPT* or *LbPT*.

Phylogenetic analysis of RIPT and LbPT

The deduced *RIPT* and *LbPT* proteins were compared with other fungal *PTs*, including 10 arbuscular mycorrhizal *PTs* and

21 ectomycorrhizal *PTs* (the species name, gene IDs, and accession number are shown in Table 1). *ScPHO84* (Bun-Ya et al. 1991) was also considered because of its well-known function. Two main clades were distinguished (Fig. 1), one branch for the *LbPT* and *HcPT1* and the second branch for the *RIPT*, another 20 ectomycorrhizal *PTs*, 10 arbuscular mycorrhizal *PTs*, and *ScPHO84*. *RIPT* was closely related to three *PTs* of *P. croceum*, including *PcPT1* (KIM88284, 77 % similarity), *PcPT2* (KIM78090, 76 % similarity), and *PcPT3* (KIM84110, 71 % similarity), and *LbPT* was closely related to *HcPT1* (KIM36204.1, 82 % similarity).

Functional complementation verification of RIPT and LbPT in yeast

RIPT and *LbPT* were transformed into the MB192 mutant using the pUG23 vector to examine their P transport functions. With the gradually dilution of the yeast cells, the growth of four types of yeast cells, including MB192 with empty pUG23 vector, the transformed MB192 cells with *RIPT* and *LbPT*, and the WT yeast cells with empty pUG23 vector, decreased in two YPD media with different Pi concentrations (60 and 200 $\mu\text{mol/L}$, Fig. S5). Compared with the strongly inhibited growth of MB192 yeast cells transformed with the empty pUG23 vector, *RIPT* and *LbPT* expression recovered the yeast growth using the P absorption ability of these two genes (Fig. S5a, b).

The effect of pH on the activities of RIPT and LbPT

To determine the pH dependence of *RIPT* and *LbPT*, the optical density of the yeast cell lines was measured at a range of 4.0–8.0 pH values with 80 $\mu\text{mol/L}$ of phosphate. The growth of MB192+*RIPT* and MB192+*LbPT* strains was similar to that of the WT yeast strain, but the growth of the control MB192 strain with the empty pUG23 vector was significantly inhibited under all of the tested pH levels (Fig. 2). In addition, four types of yeast strain exhibited the best growth under pH=6, and their growth was repressed when the pH value exceeded 6. These results suggested that both the *RIPT* and *LbPT* were H⁺-transporters. Subsequently, the growth curves of the four yeast mutants (MB192+eV, MB192+*RIPT*, MB192+*LbPT*, and WT+eV) were determined at the optimal pH value (pH=6, Fig. S6).

Subcellular localization of RIPT and LbPT in yeast

In contrast to the dispersive distribution of GFP proteins in transformed MB192 yeast with the empty vectors pUG23+*GFP* (Fig. 3a), *GFP*+*RIPT* (Fig. 3b), and *GFP*+*LbPT* (Fig. 3c), fusion protein expressions were restricted to the plasma membrane in the transformed yeast cells. These findings were consistent with the subcellular localization

Table 1 Gene IDs and accession numbers of the mycorrhizal fungal PTs used in Fig. 1

Species	Gene IDs	Accession numbers	References
<i>Amanita muscaria</i>	<i>AmPT1</i>	KIL57367	Casieri et al. (2013)
	<i>AmPT2</i>	KIL58048	
	<i>AmPT3</i>	KIL67497	
<i>Boletus edulis</i>	<i>BePT</i>	JX524166	Wang et al. (2014)
<i>Diversispora epigaea</i>	<i>DePT</i>	U38650.1	Harrison and van Buuren (1995)
<i>Funneliformis coronatum</i>	<i>FcPT</i>	GU585499.1	Sokolski et al. (2011)
<i>Funneliformis mosseae</i>	<i>FmPT</i>	DQ074452.1	Benedetto et al. (2005)
<i>Glomus aggregatum</i>	<i>GaPT</i>	GU585518.1	Sokolski et al. (2011)
<i>Hebeloma cylindrosporum</i>	<i>HcPT1</i>	AJ970310.1	Tatry et al. (2009)
	<i>HcPT2</i>	KIM36204.1	
<i>Laccaria bicolor</i>	<i>LabPT</i>	XM_001880935.1	Martin et al. (2008)
<i>Leucocortinarius bulbiger</i>	<i>LbPT</i>	KM594557	–
<i>Paxillus involutus</i>	<i>PiPT1</i>	KIJ14228	Casieri et al. (2013)
	<i>PiPT2</i>	KIJ14228	
<i>Paxillus rubicundulus</i>	<i>PrPT</i>	KIK90461	Casieri et al. (2013)
<i>Piloderma croceum</i>	<i>PcPT1</i>	KIM88284	Casieri et al. (2013)
	<i>PcPT2</i>	KIM78090	
	<i>PcPT3</i>	KIM84110	
<i>Pisolithus microcarpus</i>	<i>PmPT</i>	KIK25030	Casieri et al. (2013)
<i>Pisolithus tinctorius</i>	<i>PtPT</i>	KIO14954	Casieri et al. (2013)
<i>Pholiota nameko</i>	<i>PnPT</i>	AB060641.1	Tasaki et al. (2002)
<i>Rhizophagus clarum</i>	<i>RhcPT</i>	GU585521.1	Sokolski et al. (2011)
<i>Rhizophagus custos</i>	<i>RhcuPT</i>	GU585522.1	Sokolski et al. (2011)
<i>Rhizophagus diaphanus</i>	<i>RhdPT</i>	GU585519.1	Sokolski et al. (2011)
<i>Rhizophagus intraradices</i>	<i>RhiPT</i>	AF359112.1	Maldonado-Mendoza et al. (2001)
<i>Rhizophagus irregulare</i>	<i>RhirPT</i>	GU585503.1	Sokolski et al. (2011)
<i>Rhizophagus proliferus</i>	<i>RhpPT</i>	GU585523.1	Sokolski et al. (2011)
<i>Rhizopogon luteolus</i>	<i>RIPT</i>	KM594556	–
<i>Saccharomyces cerevisiae</i>	<i>ScPHO84</i>	D90346	Bun-Ya et al. (1991)
<i>Scleroderma citrinum</i>	<i>ScPT</i>	KIM62761	Casieri et al. (2013)
<i>Suillus luteus</i>	<i>SIPT1</i>	KIK45244	Casieri et al. (2013)
	<i>SIPT2</i>	KIK37879	
<i>Tuber melanosporum</i>	<i>TmPT</i>	XM_002837842.1	Martin et al. (2010)
<i>Tulasnella calospora</i>	<i>TcPT</i>	KIO31765	Casieri et al. (2013)

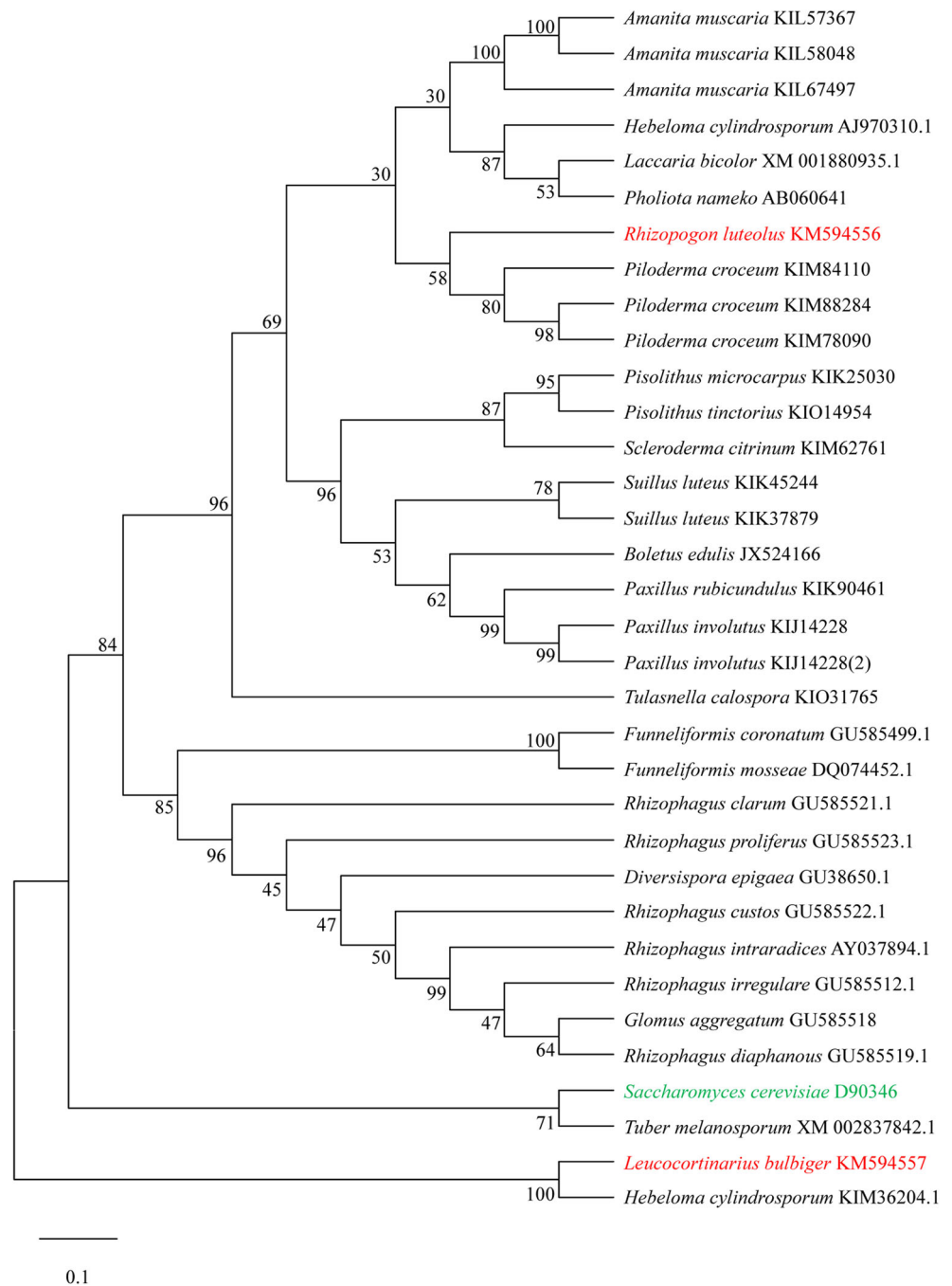
prediction in the plasma membrane of the online WoLF PSORT (Horton et al. 2007) protein predictor (In the predicted results, RIPT and LbPT have maximum likelihood with the plasma membrane protein ScPHO84, 44.14 % for the RIPT and 31.41 % for the LbPT).

The acid phosphatase enzyme activities of RIPT and LbPT in yeast

In contrast to the lack of color change in the MB192 yeast strain with the empty pUG23 vector in 20 $\mu\text{mol/L}$ Pi supplement, and the minor color changes in 60, 100, and 200 $\mu\text{mol/L}$ Pi, bromocresol purple staining in the MB192+*RIPT* and MB192+*LbPT* yeast strains revealed an obvious color

shift from pale brown to yellow, which was similar to the color change in the WT yeast strain during the acidification of the liquid medium (Fig. S7). The acid phosphatase enzyme activities of these four types of yeast strains at different Pi concentrations are shown in Fig. 4. For all four yeast strains, the acid phosphatase enzyme activities decreased with increasing phosphate concentrations. Furthermore, the acid phosphatase enzyme activity of the MB192 mutant transformed yeast with the empty vector pUG23 (MB192+eV) was higher than the activity in the other three yeast strains. It is important to note that the P absorption ability of the MB192 strain transformed with *RIPT* and *LbPT* would recover to the same levels as the WT yeast strain.

Fig. 1 Unrooted phylogenetic tree of RIPT, LbPT, and other fungal PTs based on the maximum likelihood method. RIPT and LbPT are labeled using a *red font*, and *ScPHO84* is labeled using a *blue font*. The gene IDs and accession numbers of other fungal PTs are shown in Table 1. Values of the major clusters are indicated in the node or branch of the tree, which represents the bootstrap confidence, tested using 1000 replicates of the dataset



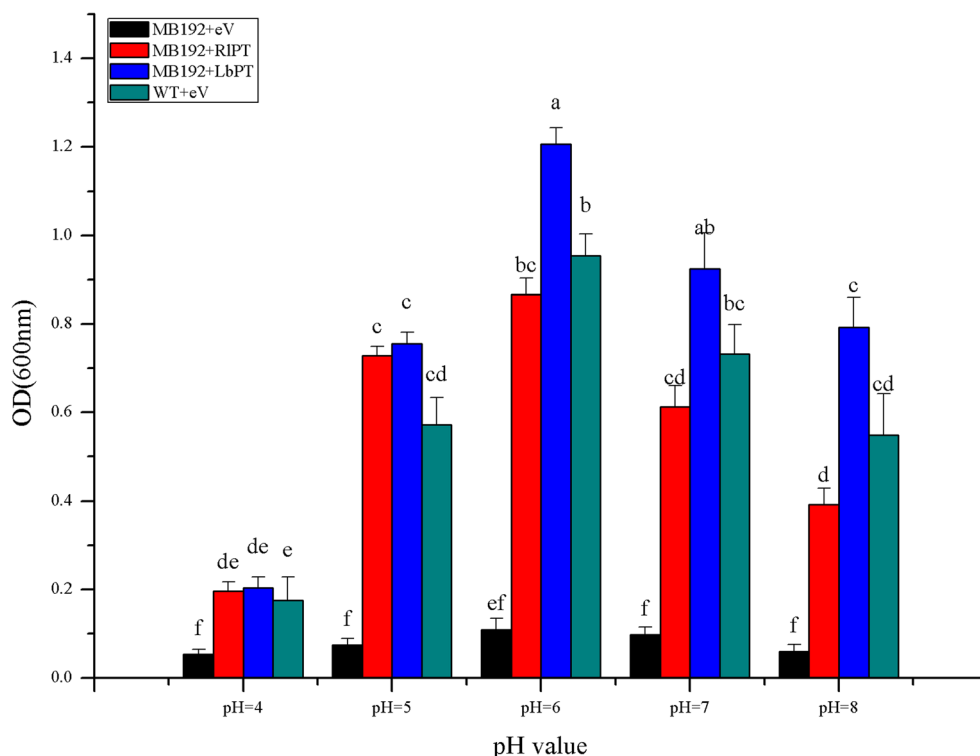
The Michaelis constant (K_m) of RIPT and LbPT

As the data show in Fig. 5, the MB192 mutant yeast can secrete an acid phosphatase enzyme, the K_m value of which is 144.79 $\mu\text{mol/L}$. However, the K_m values of the proteins encoded by the *RIPT* and *LbPT* after they were transformed into the MB192 strain were 57.90 and 35.87 $\mu\text{mol/L}$ (Fig. 5), respectively. These results indicate that the *RIPT* and *LbPT* encode for two high-affinity phosphate transporters.

The relative expression of RIPT and LbPT at different Pi concentrations

Compared with the expression levels of *RIPT* and *LbPT* in Ohta medium which added normal Pi (1 g/L), RT-PCR analysis revealed that both *RIPT* and *LbPT* were significantly up-regulated in a nutrient-deficient medium (0.01 and 0.1 g/L KH_2PO_4) and down-regulated in a nutrient-enriched medium (5 and 10 g/L KH_2PO_4 , Fig. 6). Furthermore, compared with the level of *LbPT* expression, it was clear that the *RIPT*

Fig. 2 The effects of different pH levels (4–8) on the growth (OD 600 values) of the MB192 mutant yeast strains transformed by a recombinant vector with *RIPT* (MB192+*RIPT*) and *LbPT* (MB192+*LbPT*), a WT yeast strain (WT+eV) and the MB192 mutant yeast strain (MB192+eV) transformed with empty pUG23 vector in YNB medium containing 80 $\mu\text{mol/L}$ of phosphate at 30 °C and at 180 rpm for 24 h. Different lowercase letters above the error bars indicate samples that differ significantly from each other: Duncan's multiple range tests at the 5 % level ($n = 5$)



expression showed an increasing tendency under the same Pi concentration (e.g., the relative expression of *RIPT* in 0.01 g/L of KH_2PO_4 of Ohta medium was 72.36, whereas it was 60.23 for *LbPT*).

Discussion

The low concentration of available Pi in the soil (Marschner and Rimmington 1988) is a major challenge faced by all plants (Nussaume et al. 2011). Fortunately, mycorrhizal fungi can help most plants absorb Pi using external mycelia (Facelli et al. 2014), a process governed by fungal high-affinity PTs (Bucher 2007). In the present study, two PTs were isolated, identified, and functionally characterized in *R. luteolus* and *L. bulbiger*, which form symbiotic ectomycorrhizae with *P. tabulaeformis*. For ECM fungi, many genes encoding ECM fungal PTs have been identified (Casieri et al. 2013; Wang et al. 2014). Among all PTs identified thus far in ECM fungi, few PTs, such as *HcPT1*, *HcPT2* (Tatry et al. 2009), and *BePT* (Wang et al. 2014), have been characterized by yeast complementation (The main properties, including ORF length, predicted molecular weight, predicted isoelectric point, hydrophobicity/hydrophilicity, transmembrane regions, optimal pH, and K_m values of these genes are listed in Table S2).

The homology analysis revealed that *RIPT* and *LbPT* were highly homologous to other ectomycorrhizal PTs, including 77 % similarity to the *PcPT1* protein in *RIPT*, 81 % identity

with *HcPT1* (Tatry et al. 2009) in *LbPT*, and 68 % of *RIPT* amino acids identity with the *BePT* (Wang et al. 2014). In addition, the variation of five identified ECM PTs' ORF length is very small (Table S2). The two full lengths of PT

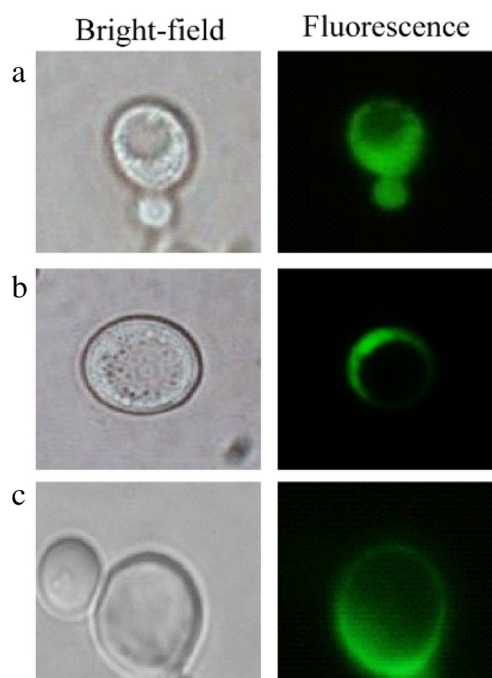


Fig. 3 Bright-field (left) and fluorescence (right) microscopy images of GFP fusion proteins expressed in the MB192 mutant yeast transformed with pUG23+*GFP* harboring no insert (empty) (a), *GFP+RIPT* transformation (b), and *GFP+LbPT* transformation (c)

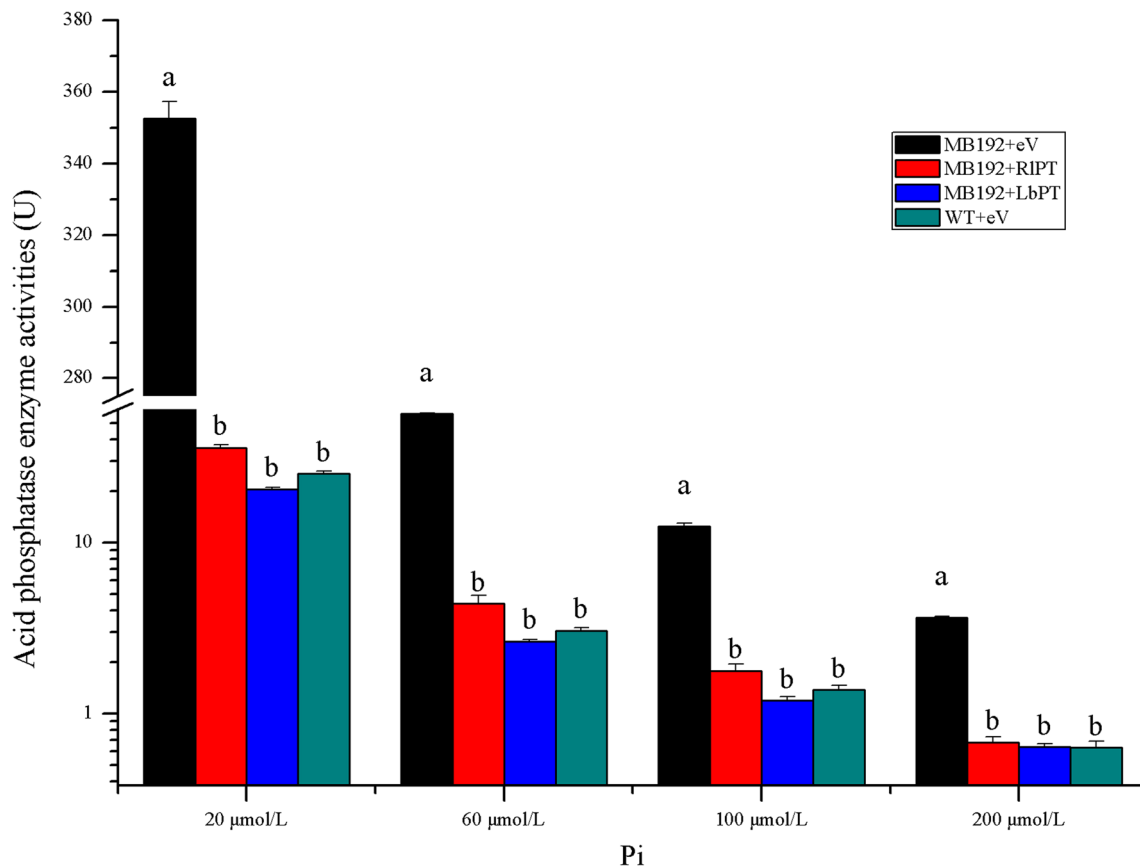


Fig. 4 The acid phosphatase enzyme activities of the MB192 mutant yeast transformed with the empty vector pUG23 (MB192+eV), pUG23+*RIPT* (MB192+RIPT), and pUG23+*LbPT* (MB192+LbPT) and WT yeast transformed with the empty vector pUG23 (WT+eV). All aliquots were cultivated in tubes containing 20, 60, 100, and 200 µmol/L of phosphatase YNB medium (pH=4.8) at 30 °C and at 180 rpm for

24 h. The values of the lower vertical coordinate are the Lg (acid phosphatase enzyme activity). In the same phosphatase concentration YNB medium, *different lowercase letters above the error bars* indicate samples that differ significantly from each other: Duncan's multiple range tests at the 5 % level ($n=5$)

cDNAs, named *HcPT1* and *HcPT2*, are 1647 and 1686 bp long, respectively (Tatry et al. 2009); the ORF length of *BePT* is 1629 bp (Wang et al. 2014); and the data for *RIPT* and *LbPT* are 1653 and 1680 bp, respectively. These results indicated that

ECM *PTs* are highly conserved throughout evolution and share high protein sequence identities.

The *PT* proteins are present in most living organisms and are usually divided into H^+ - (Pht1) and Na^+ -dependent (Pht2) transporters (Casieri et al. 2013; Ravera et al. 2007). Many

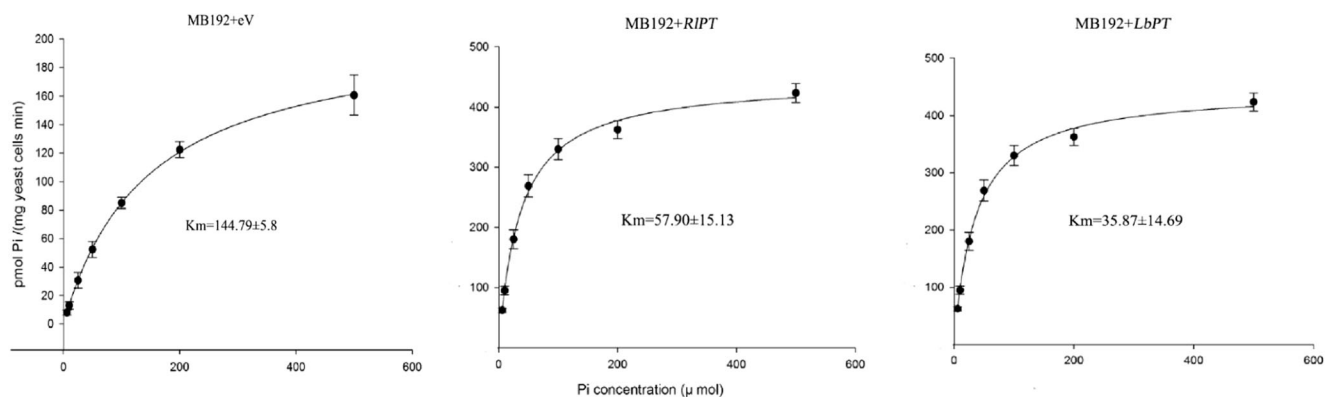
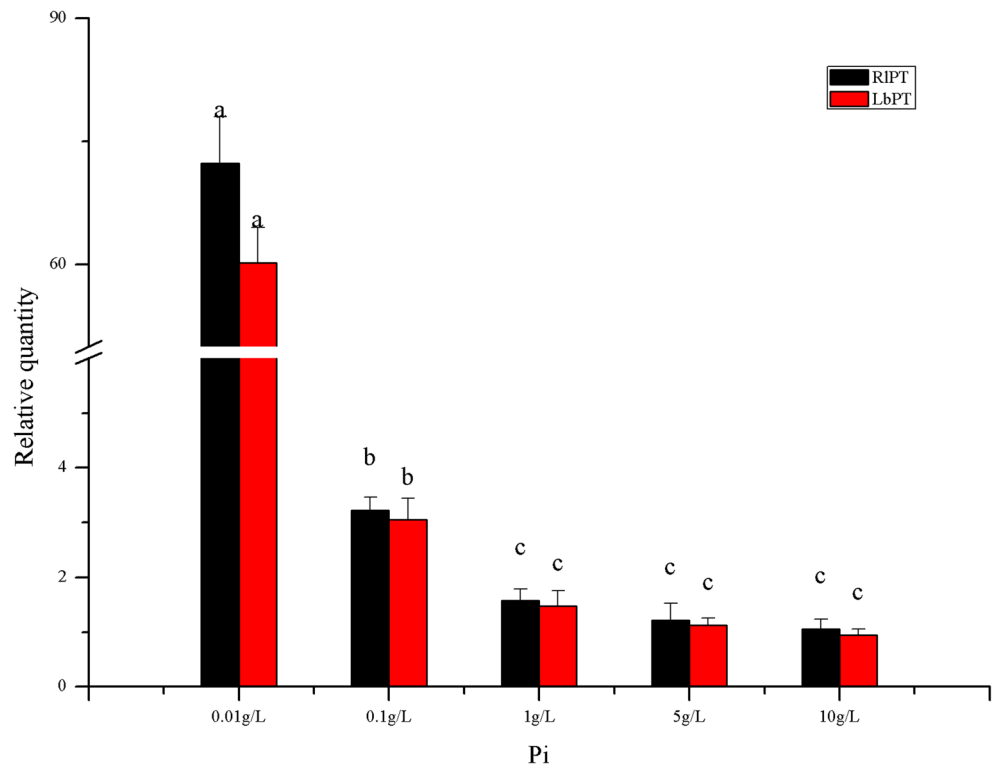


Fig. 5 The P uptake kinetic curves of the MB192 mutant yeast transformed with the empty vector pUG23 (MB192+eV), pUG23+*RIPT* (MB192+RIPT), and pUG23+*LbPT* (MB192+LbPT)

Fig. 6 Relative expression of *RIPT* and *LbPT* measured by RT-PCR in mycelium cultured in Ohta medium with normal Pi (1 g/L of KH_2PO_4), nutrient-enriched (5 and 10 g/L), and nutrient-deficient (0.01 and 0.1 g/L) conditions. The gene expression of these two *PTs* was normalized against an internal reference gene, γ -actin



fungal *PTs* are recognized as *Pht2* transporters (Ai et al. 2009), but for the ECM fungi, most of these transporters belong to the *Pht1* subfamily (Pi:H^+ transporters), except for *TmPT3*, which encodes a *PT* that clusters with Pi:Na^+ transporters (Casieri et al. 2013). The predicted products of *RIPT* and *LbPT* consisted of 10 and 9 trans-membrane domains, respectively, which were separated into two groups connected with a hydrophilic loop. In addition, the amino acid sequences of *RIPT* and *LbPT* include the signature sequence GGDYPLSATIxSE (data not shown); these structural arrangements are typical for *Pht1* transporters (Karandashov and Bucher 2005; Liu et al. 2014). The uptake of *Pi* by the members of the *Pht1* family is generally accompanied by an increase in the extracellular pH and an acidification of the cytoplasm (DiTusa et al. 2015; Pedersen et al. 2013). The optimal pH value of the MB192 mutant yeast transformed with the pUG23+*RIPT* and pUG23+*LbPT* is 6, and the subcellular localization of *RIPT* and *LbPT* (Fig. 3) indicated that these two genes were expressed in the plasma membrane. Based on the two genes' sequences, optimal pH value of transformed yeast cells, and subcellular localization results, we confirmed that *RIPT* and *LbPT* encode the Pi:H^+ transporter.

Several approaches have been used to investigate the *Pi* transport properties of the various *Pht1* family members (Glassop et al. 2005; Kobae and Hata 2010). In the current study, *RIPT* and *LbPT* were able to complement the loss of the high-affinity *Pi* transporter activity of the MB192 yeast mutant. The K_m values of *RIPT* and *LbPT* were 57.9 and 35.7 $\mu\text{mol/L Pi}$, respectively, values that are in the high-

affinity concentration range (Fig. 5). To the best of our knowledge, only three mycorrhizal *PTs* K_m have been measured by this method, including *HcPT1* (5 $\mu\text{mol/L}$, Taty et al. (2009)), *DePT* (18 $\mu\text{mol/L}$, Harrison and van Buuren (1995)), and *HcPT2* (55 $\mu\text{mol/L}$, Taty et al. (2009)). The K_m of *RIPT* lies outside of the K_m range of other mycorrhizal high-affinity *PTs*, but these data lie within the K_m range of most *Pht1* high-affinity *PTs*, e.g., *MtPT5* (13 $\mu\text{mol/L}$, *Medicago truncatula*, Liu et al. (2008)), *PtPT6* (22.6 $\mu\text{mol/L}$, *Populus trichocarpa*, Loth-Pereda et al. (2011)), *CmPT1* (35.2 $\mu\text{mol/L}$, *Chrysanthemum morifolium*, Liu et al. (2014)), *GmPT1* (68.9 $\mu\text{mol/L}$, *Glycine max*, Fan et al. (2013)), and *OsPT6* (97 $\mu\text{mol/L}$, *Oryza sativa*, Ai et al. (2009)).

As shown in Fig. 1, *RIPT*, *LbPT*, and the other 32 fungal *PTs* (31 mycorrhizal *PTs* and *ScPHO84*) can be distinguished in 2 branches by phylogenetic analysis, one branch for the *LbPT* and *HcPT1* and the second branch for the *RIPT*, another 20 ECM *PTs*, 10 AM *PTs*, and *ScPHO84*. The second branch also can be divided into 3 small clades, one clade for the 20 ECM *PTs* (*RIPT* in this clade), the second clade for 10 AM *PTs*, and the last clade for the *TcPT*. The phylogenetic analyses of all mycorrhizal *PTs* used in present study were basically consistent with the traditional morphological classification of mycorrhizal fungi and *L. bulbiger* is most closely related to *H. cylindrosporium*, whereas *R. luteolus* is most closely related to *P. croceum*.

In the present study, both *RIPT* and *LbPT* were up-regulated in their mycelia under *Pi* starvation conditions. Also, *R. luteolus* and *L. bulbiger* were the two most efficient ECM

fungi for *P. tabulaeformis* in Pi absorption and inoculation effects among five species (*L. bulbiger*, *R. luteolus*, *Suillus grevillei*, *Tricholoma fulvum*, and *Tricholoma terreum*) of ECM fungi when *P. tabulaeformis* seedlings were inoculated with these fungal strains (Bai et al. 2009). These research results presumably explain why *P. tabulaeformis* exhibits high dependence on ectomycorrhizae at the P depletion area in the natural forest ecosystems of northern China.

Conclusion

In conclusion, *RIPT* and *LbPT* encode for two typical high-affinity phosphate transporter in *R. luteolus* and *L. bulbiger*. *RIPT* and *LbPT* are expected to encode the polypeptide with 550 and 559 amino acid residues, respectively. The pI and the calculated molecular mass are 8.376 and 59.786 kDa for *RIPT* and 7.190 and 61.26 kDa for *LbPT*. These two proteins are the hydrophobic protein, *RIPT* exhibits 10 TMs but *LbPT* consists of 9 TMs. *RIPT* is closely related to *PcPT1*, and *LbPT* is closely related to *HePT1*. *RIPT* and *LbPT* might function in a wide range of Pi environments (0.01 to 10 g/L KH_2PO_4 in Ohta medium) and presumably play an important role in phosphate acquisition by *P. tabulaeformis* under natural conditions.

Acknowledgments This work was supported by the National Natural Science Foundation of China (Nos. 31060110 and 31360125). We would like to express our appreciation to Prof. J. Hegemann (Institut für Mikrobiologie, Heinrich-Heine-Universität Düsseldorf, Germany) for generously providing the yeast mutants (MB192) and two types of vectors (pUG23 and pUG23+*GFP*).

References

- Ai P, Sun S, Zhao J, Fan X, Xin W, Guo Q, Yu L, Shen Q, Wu P, Miller AJ (2009) Two rice phosphate transporters, OsPht1:2 and OsPht1:6, have different functions and kinetic properties in uptake and translocation. *Plant J* 57:798–809. doi:10.1111/j.1365-313X.2008.03726.x
- Bai S-L, Li G-L, Liu Y, Dumroese RK, Lv R-H (2009) *Ostryopsis davidiana* seedlings inoculated with ectomycorrhizal fungi facilitate formation of mycorrhizae on *Pinus tabulaeformis* seedlings. *Mycorrhiza* 19:425–434. doi:10.1007/s00572-009-0245-2
- Benedetto A, Magurno F, Bonfante P, Lanfranco L (2005) Expression profiles of a phosphate transporter gene (*GmosPT*) from the endomycorrhizal fungus *Glomus mosseae*. *Mycorrhiza* 15:620–627. doi:10.1007/s00572-005-0006-9
- Boon N, Goris J, De Vos P, Verstraete W, Top EM (2000) Bioaugmentation of activated sludge by an indigenous 3-chloroaniline-degrading *Comamonas testosteroni* strain, 12gfp. *Appl Environ Microbiol* 66:2906–2913. doi:10.1128/AEM.66.7.2906-2913.2000
- Bucher M (2007) Functional biology of plant phosphate uptake at root and mycorrhiza interfaces. *New Phytol* 173:11–26. doi:10.1111/j.1469-8137.2006.01935.x
- Bun-Ya M, Nishimura M, Harashima S, Oshima Y (1991) The PHO84 gene of *Saccharomyces cerevisiae* encodes an inorganic phosphate transporter. *Mol Cell Biol* 11:3229–3238. doi:10.1128/MCB.11.6.3229
- Casieri L, Lahmidi NA, Doidy J, Veneault-Fourrey C, Migeon A, Bonneau L, Courty P-E, Garcia K, Charbonnier M, Delteil A (2013) Biotrophic transportome in mutualistic plant–fungal interactions. *Mycorrhiza* 23:597–625. doi:10.1007/s00572-013-0496-9
- Chandra J, Kuhn DM, Mukherjee PK, Hoyer LL, McCormick T, Ghannoum MA (2001) Biofilm formation by the fungal pathogen *Candida albicans*: development, architecture, and drug resistance. *J Bacteriol* 183:5385–5394. doi:10.1128/JB.183.18.5385-5394.2001
- Chen K, Abbott RJ, Milne RI, Tian XM, Liu J (2008) Phylogeography of *Pinus tabulaeformis* Carr. (Pinaceae), a dominant species of coniferous forest in northern China. *Mol Ecol* 17:4276–4288. doi:10.1111/j.1365-294X.2008.03911.x
- Classics-Barka T, Anderson P (1962) Histochemical methods for acid phosphatase using hexazonium pararosanalin as coupler. *J Histochem Cytochem* 10:741–753
- Cormack BP, Bertram G, Egerton M, Gow NA, Falkow S, Brown AJ (1997) Yeast-enhanced green fluorescent protein (yEGFP): a reporter of gene expression in *Candida albicans*. *Microbiology* 143:303–311. doi:10.1099/00221287-143-2-303
- de Campos MC, Pearse SJ, Oliveira RS, Lambers H (2013) *Viminaria juncea* does not vary its shoot phosphorus concentration and only marginally decreases its mycorrhizal colonization and cluster-root dry weight under a wide range of phosphorus supplies. *Ann Bot* 111:801–809. doi:10.1093/aob/mct035
- DiTusa SF, Fontenot EB, Wallace RW, Silvers MA, Steele TN, Elnagar AH, Dearman KM, Smith AP (2015) A member of the phosphate transporter 1 (Pht1) family from the arsenic-hyperaccumulating fern *Pteris vittata* is a high-affinity arsenate transporter. *New Phytologist*. doi:10.1111/nph.13472
- Faber KN, Haima P, Harder W, Veenhuis M, Geert A (1994) Highly-efficient electrotransformation of the yeast *Hansenula polymorpha*. *Curr Genet* 25:305–310. doi:10.1007/BF00351482
- Facelli E, Duan T, Smith SE, Christophersen HM, Facelli JM, Smith FA (2014) Opening the black box: outcomes of interactions between arbuscular mycorrhizal (AM) and non-host genotypes of *Medicago* depend on fungal identity, interplay between P uptake pathways and external P supply. *Plant Cell Environ* 37:1382–1392. doi:10.1111/pce.12237
- Fan C, Wang X, Hu R, Wang Y, Xiao C, Jiang Y, Zhang X, Zheng C, Fu Y-F (2013) The pattern of phosphate transporter 1 genes evolutionary divergence in *Glycine max* L. *BMC Plant Biol* 13:48. doi:10.1186/1471-2229-13-48
- Faustino LI, Bulfe NM, Pinazo MA, Monteoliva SE, Graciano C (2013) Dry weight partitioning and hydraulic traits in young *Pinus taeda* trees fertilized with nitrogen and phosphorus in a subtropical area. *Tree Physiol* 33:129. doi:10.1093/treephys/tps129
- Glassop D, Smith SE, Smith FW (2005) Cereal phosphate transporters associated with the mycorrhizal pathway of phosphate uptake into roots. *Planta* 222:688–698. doi:10.1007/s00425-005-0015-0
- Harrison MJ, van Buuren ML (1995) A phosphate transporter from the mycorrhizal fungus *Glomus versiforme*. *Nature* 378:626–629. doi:10.1038/378626a0
- Hinsinger P (2001) Bioavailability of soil inorganic P in the rhizosphere as affected by root-induced chemical changes: a review. *Plant Soil* 237:173–195. doi:10.1023/A:1013351617532
- Horton P, Park KJ, Obayashi T, Fujita N, Harada H, Adams-Collier CJ, Nakai K (2007) WoLF PSORT: protein localization predictor. *Nucleic Acids Res* 35(suppl 2):W585–W587. doi:10.1093/nar/gkm259
- Karandashov V, Bucher M (2005) Symbiotic phosphate transport in arbuscular mycorrhizas. *Trends Plant Sci* 10:22–29. doi:10.1016/j.plants.2004.12.003

- Kobae Y, Hata S (2010) Dynamics of periarbuscular membranes visualized with a fluorescent phosphate transporter in arbuscular mycorrhizal roots of rice. *Plant Cell Physiol* 51:341–353. doi:10.1093/pcp/pcq013
- Liu J, Versaw WK, Pumplun N, Gomez SK, Blaylock LA, Harrison MJ (2008) Closely related members of the *Medicago truncatula* PHT1 phosphate transporter gene family encode phosphate transporters with distinct biochemical activities. *J Biol Chem* 283:24673–24681. doi:10.1074/jbc.M802695200
- Liu P, Chen S, Song A, Zhao S, Fang W, Guan Z, Liao Y, Jiang J, Chen F (2014) A putative high affinity phosphate transporter, CmPT1, enhances tolerance to Pi deficiency of chrysanthemum. *BMC Plant Biol* 14:18. doi:10.1186/1471-2229-14-18
- Livak KJ, Schmittgen TD (2001) Analysis of relative gene expression data using real-time quantitative PCR and the $2^{-\Delta\Delta CT}$ method. *Methods* 25:402–408. doi:10.1006/meth.2001.1262
- Loth-Pereda V, Orsini E, Courty P-E, Lota F, Kohler A, Diss L, Blaudez D, Chalot M, Nehls U, Bucher M (2011) Structure and expression profile of the phosphate Pht1 transporter gene family in mycorrhizal *Populus trichocarpa*. *Plant Physiol* 156:2141–2154. doi:10.1104/pp.111.180646
- Maldonado-Mendoza IE, Dewbre GR, Harrison MJ (2001) A phosphate transporter gene from the extra-radical mycelium of an arbuscular mycorrhizal fungus *Glomus intraradices* is regulated in response to phosphate in the environment. *Mol Plant Mic Interact* 14:1140–1148. doi:10.1094/MPMI.2001.14.10.1140
- Mao X-L (2009) *Macromycetes of China*. Science Press, Beijing
- Marschner H, Rimmington G (1988) Mineral nutrition of higher plants. *Plant Cell Environ* 11:147–148. doi:10.1111/j.1365-3040.1988.tb01130.x
- Martin F, Aerts A, Ahrén D, Brun A, Danchin E, Duchaussoy F, Gibon J, Kohler A, Lindquist E, Pereda V (2008) The genome of *Laccaria bicolor* provides insights into mycorrhizal symbiosis. *Nature* 452:88–92. doi:10.1038/nature06556
- Martin F, Kohler A, Murat C, Balestrini R, Coutinho PM, Jaillon O, Montanini B, Morin E, Noel B, Percudani R (2010) Périgord black truffle genome uncovers evolutionary origins and mechanisms of symbiosis. *Nature* 464:1033–1038. doi:10.1038/nature08867
- Melikant B, Giuliani C, Halbmayer-Watzina S, Limmongkon A, Heberle-Bors E, Wilson C (2004) The *Arabidopsis thaliana* MEK AtMKK6 activates the MAP kinase AtMPK13. *FEBS Lett* 576:5–8. doi:10.1016/j.febslet.2004.08.051
- Miransari M, Mackenzie A (2011) Development of a soil N test for fertilizer requirements for wheat. *J Plant Nutr* 34:762–777. doi:10.1080/01904167.2011.540922
- Murshudov GN, Vagin AA, Dodson EJ (1997) Refinement of macromolecular structures by the maximum-likelihood method. *Acta Cryst D* 53:240–255. doi:10.1107/S0907444996012255
- Nussaume L, Kanno S, Javot H, Marin E, Pochon N, Ayadi A, Nakanishi TM, Thibaud M-C (2011) Phosphate import in plants: focus on the PHT1 transporters. *Front Plant Sci* 30:83. doi:10.3389/fpls.2011.00083
- Ohta A (1990) A new medium for mycelial growth of mycorrhizal fungi. *Trans Mycol Soc Jpn* 31:323–334
- Pedersen BP, Kumar H, Waight AB, Risenmay AJ, Roe-Zurz Z, Chau BH, Schlessinger A, Bonomi M, Harries W, Sali A (2013) Crystal structure of a eukaryotic phosphate transporter. *Nature* 496:533–536. doi:10.1038/nature12042
- Rausch C, Bucher M (2002) Molecular mechanisms of phosphate transport in plants. *Planta* 216:23–37. doi:10.1007/s00425-002-0921-3
- Ravera S, Virkki LV, Murer H, Forster IC (2007) Deciphering PiT transport kinetics and substrate specificity using electrophysiology and flux measurements. *Am J Physiol Cell Physiol* 293:C606–C620. doi:10.1152/ajpcell.00064.2007
- Roy M, Rochet J, Manzi S, Jargeat P, Gryta H, Moreau PA, Gardes M (2013) What determines *Alnus*-associated ectomycorrhizal community diversity and specificity? A comparison of host and habitat effects at a regional scale. *New Phytol* 198:1228–1238. doi:10.1111/nph.12212
- Sezonov G, Joseleau-Petit D, D’Ari R (2007) *Escherichia coli* physiology in Luria-Bertani broth. *J Bacteriol* 189:8746–8749. doi:10.1128/JB.01368-07
- Smith SE, Read DJ (2008) *Mycorrhizal symbiosis*. Academic, New York
- Smith SE, Smith FA (2012) Fresh perspectives on the roles of arbuscular mycorrhizal fungi in plant nutrition and growth. *Mycologia* 104:1–13. doi:10.3852/11-229
- Sokolski S, Dalpé Y, Piché Y (2011) Phosphate transporter genes as reliable gene markers for the identification and discrimination of arbuscular mycorrhizal fungi in the genus *Glomus*. *Appl Environ Microbiol* 77:1888–1891. doi:10.1128/AEM.00919-10
- Stonor RN, Smith SE, Manjarrez M, Facelli E, Smith FA (2014) Mycorrhizal responses in wheat: shading decreases growth but does not lower the contribution of the fungal phosphate uptake pathway. *Mycorrhiza* 1–8. doi:10.1007/s00572-014-0556-9
- Tamura K, Peterson D, Peterson N, Stecher G, Nei M, Kumar S (2011) MEGA5: molecular evolutionary genetics analysis using maximum likelihood, evolutionary distance, and maximum parsimony methods. *Mol Biol Evol* 28:2731–2739. doi:10.1093/molbev/msr121
- Tasaki Y, Kamiya Y, Azwan A, Hara T, Joh T (2002) Gene expression during Pi deficiency in *Pholiota nameko*: accumulation of mRNAs for two transporters. *Biosci Biotechnol Biochem* 66:790–800. doi:10.1271/bbb.66.790
- Tatry MV, El Kassis E, Lambilliotte R, Corratgé C, Van Aarle I, Amenc LK, Alary R, Zimmermann S, Sentenac H, Plassard C (2009) Two differentially regulated phosphate transporters from the symbiotic fungus *Hebeloma cylindrosporum* and phosphorus acquisition by ectomycorrhizal *Pinus pinaster*. *Plant J* 57:1092–1102. doi:10.1111/j.1365-313X.2008.03749.x
- Thompson JD, Gibson TJ, Plewniak F, Jeanmougin F, Higgins DG (1997) The CLUSTAL_X windows interface: flexible strategies for multiple sequence alignment aided by quality analysis tools. *Nucl Acids Res* 25:4876–4882. doi:10.1093/nar/25.24.4876
- Tusnady GE, Simon I (2001) The HMMTOP transmembrane topology prediction server. *Bioinformatics* 17:849–850. doi:10.1093/bioinformatics/17.9.849
- Vance CP, Uhde-Stone C, Allan DL (2003) Phosphorus acquisition and use: critical adaptations by plants for securing a nonrenewable resource. *New Phytol* 157:423–447. doi:10.1046/j.1469-8137.2003.00695.x
- Wang J, Li T, Wu X, Zhao Z (2014) Molecular cloning and functional analysis of a H⁺-dependent phosphate transporter gene from the ectomycorrhizal fungus *Boletus edulis* in southwest China. *Fungal Biol* 118:453–461. doi:10.1016/j.funbio.2014.03.003
- Wu B, Watanabe I, Hayatsu M, Nioh I (1999) Effect of ectomycorrhizae on the growth and uptake and transport of ¹⁵N-labeled compounds by *Pinus tabulaeformis* seedlings under water-stressed conditions. *Biol Fert Soils* 28:136–138. doi:10.1007/s003740050474
- Wu Z, Zhao J, Gao R, Hu G, Gai J, Xu G, Xing H (2011) Molecular cloning, characterization and expression analysis of two members of the Pht1 family of phosphate transporters in *Glycine max*. *PLoS One* 6:e19752. doi:10.1371/journal.pone.0019752
- Yan X, Wu P, Ling H, Xu G, Xu F, Zhang Q (2006) Plant nutriomics in China: an overview. *Ann Bot* 98:473–482. doi:10.1093/aob/mcl116
- Zhang H-H, Tang M, Chen H, Zheng C-L (2010) Effects of inoculation with ectomycorrhizal fungi on microbial biomass and bacterial functional diversity in the rhizosphere of *Pinus tabulaeformis* seedlings. *Eur J Soil Biol* 46:55–61. doi:10.1016/j.ejsobi.2009.10.005
- Zheng R, Wang J-G, L-h T, Bai S-L, Niu Y-F (2014) Cloning and expression analysis of γ -actin gene from *Rhizopogon luteolus*. *Sci Sinicae* 50:80–85
- Zinser E, Sperka-Gottlieb C, Fasch E-V, Kohlwein SD, Paltauf F, Daum G (1991) Phospholipid synthesis and lipid composition of subcellular membranes in the unicellular eukaryote *Saccharomyces cerevisiae*. *J Bacteriol* 173:2026–2034